Smart Structures and Systems, *Vol. 26*, *No. 6* (*2020*) *765-779*
DOI: https://doi.org/10.12989/sss.2020.26.6.765

Nonlinear dynamic analysis of a RC bridge subjected to seismic loading

Germán Nanclares[1,2a], Daniel Ambrosini[*1,2], Oscar Curadelli[1,2b] and Martín Domizio[1,2c]

[1]*Universidad Nacional de Cuyo, Facultad de Ingeniería, Mendoza, Argentina*
[2]*CONICET, National Research Council, Argentina*

(*Received March 4, 2020, Revised September 8, 2020, Accepted October 6, 2020*)

Abstract. Collapse of bridges in recent earthquakes demonstrates the need to deepen the understanding of the behaviour of these structures against seismic actions. This paper presents a highly detailed numerical model of an actual bridge subjected to extreme seismic action which results in its collapse. Normally, nonlinear numerical models have high difficulties to achieve convergence when reinforced concrete is intended to be represented. The main objective of this work is to determine the efficiency of different passive control strategies to prevent the structural collapse of an existing bridge. Metallic dampers and seismic isolation by decoupling the mass were evaluated. The response is evaluated not only in terms of reduction of displacements, but also in increasing of shear force and axial force in key elements, which can be a negative characteristic of the systems studied. It can be concluded that the use of a metallic damper significantly reduces the horizontal displacements and ensures the integrity of the structure from extreme seismic actions. Moreover, the isolation of the deck, which in principle seems to be the most effective solution to protect existing bridges, proves inadequate for the case analysed due to its dynamic characteristics and its particular geometry and an unpredictable type of axial pounding in the columns. This unexpected effect on the isolation system would have been impossible to identify with simplified models.

Keywords: reinforced concrete; bridge; control vibration; nonlinear dynamic analysis; explicit FEM

1. Introduction

Earthquakes are one of the most important causes of bridge collapses. During the last decades, major earthquakes have left a balance of thousands of casualties, as well as enormous economic losses, associated with the collapse of bridges. Several examples can be highlighted, such as Loma Prieta 1989 (Schultz and Gastineau 2016), Northridge 1994 (Calvi *et al*. 2007), Chile 2010 (Schanack *et al*. 2012) or Central Italy 2016 (Di Sarno *et al*. 2019). Several typical failure mechanisms for bridges are detailed by Deng *et al*. (2016) such as girder/deck unseating, plastic hinges in piles and supports, soil failure and liquefaction or pounding between adjacent members.

Despite the aforementioned events, the response of bridges designed with modern criteria has been considerably better. Such is the case of the earthquakes of Christchurch 2011 (Wotherspoon *et al*. 2011) or Kaikoura 2016 (Palermo *et al*. 2017). However, there are a large number of existing bridges that need to be reviewed through reliable and detailed numerical models, jointly with experimental techniques, in order to ensure its level of structural safety. On the other hand, these comprehensive models may be necessary for the structural design of new critical bridges.

Regarding numerical models, related with the main topic of this work, there are many papers of varying complexity. Chandara *et al*. (2016) use an analytical method for moment-curvature analysis of prefabricated bridge columns subjected to seismic loading and Lee and Yun (2008) present a simplified nonlinear model for parameter identification of RC bridge piers.

At present, there is a growing trend to conduct more detailed modelling of bridges, considering the evolution of damage in concrete elements. Most of them are limited to minor specific zones, in order to estimate localize damage in the structure. In this sense, some authors evaluate the seismic response of bridges through detailed finite element models. Dulinska and Szczerba (2013) incorporate a scalar damaged elasticity model to take account for degradation of the horizontal deck, whereas the rest of the structure is modelled as linear-elastic elements. In a similar approach, Borón and Dulinska (2016) evaluate the seismic performance of a RC bridge. Other authors use multi-scale models, in which they combine different types of elements jointed through constraints conditions, with the aim of improving computational performance of their simulations. Li *et al*. (2017) model a bridge combining solid elements in areas of interest with linear beam elements to represent the parts that require less detail. Hu *et al*. (2017), analyse two bridges with this modelling technique, seeking to find local fails in columns that conduct to global collapse of the structure. Moharrami and Koutromanos (2017) generate a code of a constitutive model in LS-DYNA for representing concrete structures. On the other hand, Bi and Hao (2013) study the pounding damage phenomena on a bridge, owed

*Corresponding author, Ph.D.,
E-mail: dambrosini@uncu.edu.ar
[a] Student
[b] Ph.D., Professor
[c] Ph.D.

ISSN: 1738-1584 (Print), 1738-1991 (Online)

(a) Existing bridge located in Mendoza (Argentina)

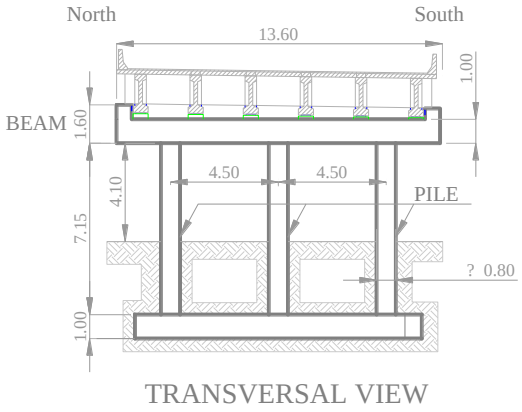

(b) Transversal view. Units in metres

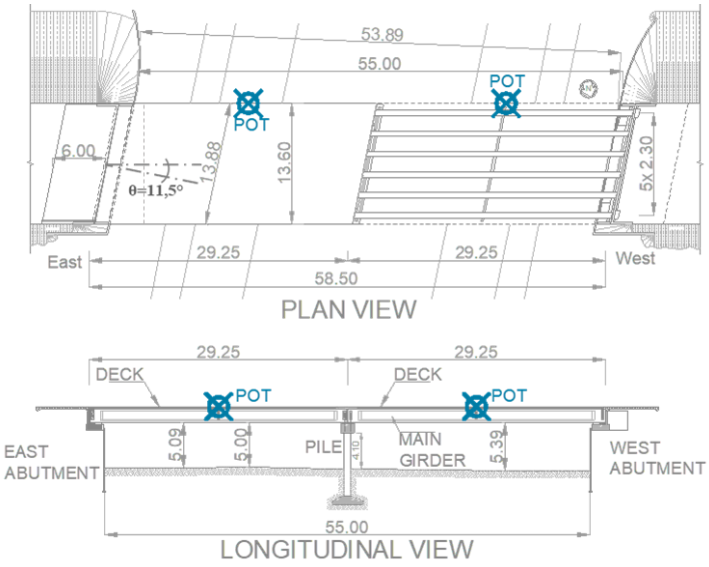

(c) Plan and longitudinal views. Units in meters

Fig. 1 Actual bridge analysed

to the impact of the girders against abutments. These same authors present a numerical study of a bridge subjected to seismic accelerations, when shear keys are incorporated in beam supports (Bi and Hao 2015). It is worth noting that these two articles use only detailed numerical meshes on specific, relatively small parts of the model, that are related to the objectives of the studies.

The main objective of this work is to determine the efficiency of different passive control strategies to prevent the structural collapse of an existing bridge through the use of a numerical model that is as realistic as possible. Moreover, as a secondary objective, the procedures and results obtained in this paper can serve as a modelling guide for the analysis of RC bridges subjected to seismic loading.

With these purposes, a full nonlinear numerical analysis of an actual bridge is carried out until collapse. Five different seismic records were used and different systems of passive control of vibration are incorporated in order to study its efficiency to prevent structural collapse. To the best of the authors' knowledge, there is no such a full detailed nonlinear model published in the technical literature, with passive control systems, that studies the complete dynamic response until collapse.

2. Description of the structure

The structure analysed is an existing bridge located in Mendoza, Argentina (Fig. 1(a)). It is a two-span bridge with post-tensioned RC girders and an intermediate support of a reinforced concrete frame that provides two independent structures of 29.25 m length each one. The middle RC frame is composed by three circular cross-section columns, 4.10 m height, jointed at the top by a rectangular beam. The road surface is a 50 mm thick asphalt layer, placed over a precast reinforced concrete deck. The aforementioned deck is discontinuous at the middle length, which is supported by six "I" RC post-tensioned beams, separated 2.30 m, simply supported at each end. Both are connected by means of steel shear-key embedded into cast in-situ concrete.

Main post-tensioned girders were built with 30 MPa strength concrete and the remaining structure with 21 MPa strength concrete. Elastomeric seat bearing was attached at both ends of each girder. The geometric characteristics of the studied bridge are presented in Figs. 1(b)-(c).

As it can be seen in Fig. 1(c), the geometry of the bridge shows an angle of 11.5° between the longitudinal axis and the one formed by the extreme supports, at the abutments.

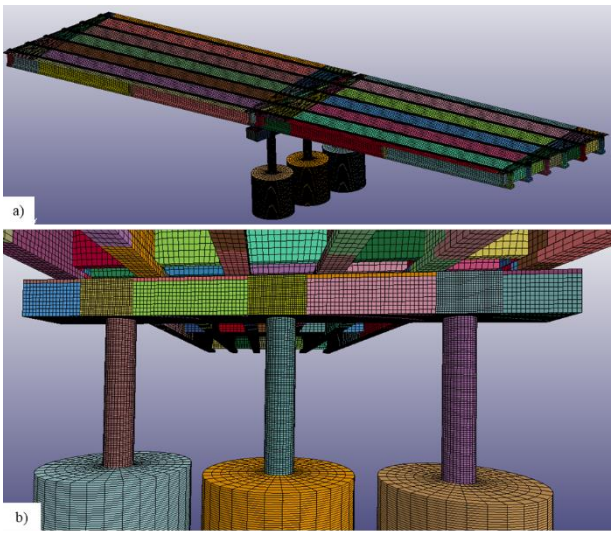

Fig. 2 (a) 3D view of the numerical model; (b) view of reinforced concrete frame at intermediate support

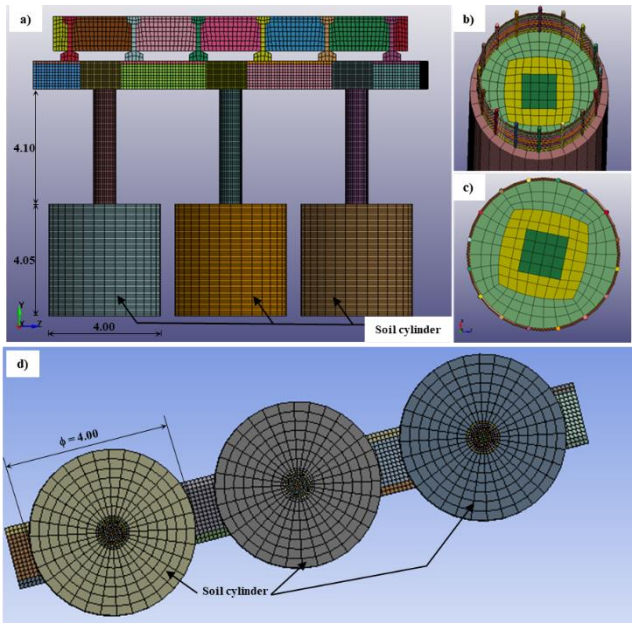

Fig. 3 (a) Finite element model; (b) steel rebars; (c) transversal section of the concrete column; (d) view of the soil cylinders. Units in meters

This skewed angle induces torsional effects (Akbari and Maalek 2018), and a rotation of the deck in its plane, when horizontal accelerations appear (He *et al*. 2012). The aforementioned rotation proceeds from the horizontal reaction provided by abutments, which act at a perpendicular angle to the contact surface. This feature may result in the reduction of the support area and consequently collapse owing to unseating of the girders (Schanack *et al*. 2012).

3. Numerical model

A detailed 3D model was carried out including RC frame, slabs and main girders (Figs. 2 and 3). Explicit finite element code LS-DYNA (LSTC 2017) is employed to calculate the non-linear seismic response of the bridge. The explicit codes offer advantages over the classic scheme of implicit solutions when it comes to represent high nonlinearities that include collapse mechanisms, which are caused by non-convergence problems, typical of implicit schemes.

Table 1 Parameters considered in numerical model of the bridge

Material	Constitutive model	Properties
Columns concrete (H21)	Winfrith + Erosion	$\rho = 2300$ kg/m^3 $f_c' = 21$ MPa $f_t' = 2.1$ MPa $E_c = 11850$ MPa Poisson's modulus = 0.18 Aggregate size = 0.0125 m Max. crack width = 0.02 mm Effective strain limit = 0.03
Slabs concrete (H21)	Elastic	$\rho = 2400$ kg/m^3 $E_c = 9000$ MPa Poisson's modulus = 0.18
Girders concrete (H30)	Winfrith + Erosion (Smeared reinf.)	$\rho = 2400$ kg/m^3 $f_c' = 30$ MPa $f_t' = 3.0$ MPa $E_c = 51500$ MPa Poisson's modulus = 0.18 Aggregate size = 0.0125 m Max. crack width = 0.02 mm Effective strain limit = 0.03
Steel reinf. Columns (ADN420)	Elastic-Plastic (Kinematic hardening)	$\rho = 7850$ kg/m^3 $f_y = 420$ MPa $E_s = 200000$ MPa $E_{Post-Yield} = 2800$ MPa Poisson's modulus = 0.30
Soil	Elastic	$\rho = 1900$ kg/m^3 $E = 240$ MPa Poisson's modulus = 0.35

Focused in the behaviour of RC frame, a highly detailed mesh was developed, considering 8-node solid hexahedral elements with a single integration point that represents concrete, and Hughes-Liu formulation beam elements to take into account the steel bars. It is assumed that the concrete and steel modelled are perfectly bonded, performed by means of merging shared nodes in the mesh (Fig. 3(b)). Longitudinal post-tensioned girders are modelled with 8-node solid hexahedral elements with a single integration point, and the horizontal deck is made with 4-node shell elements with Belytschko-Tsay formulation. The typical size of the elements in the RC frame, as in the beam-column joint, is 50 mm. The remainder of the head girder is modelled with 100 mm solid elements. The longitudinal beams are modelled with 250 mm elements, except at the ends, where the size is reduced in half. The beam elements that represent the steel reinforcement, which share nodes with the adjacent solid elements, have identical dimensions. The entire 3D model is depicted in Fig. 2 and some details are shown in Fig. 3.

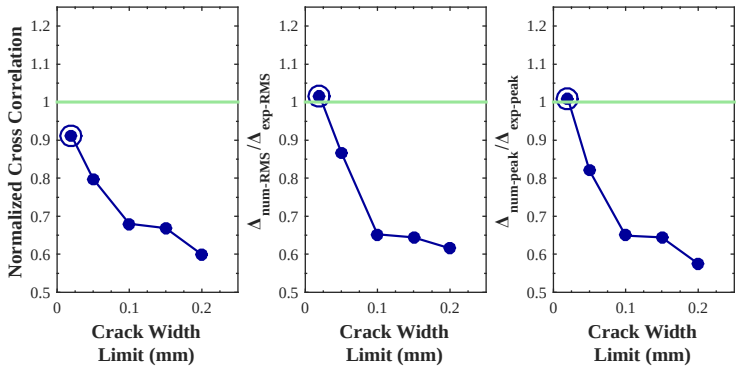

Fig. 4 Comparison indicators of experimental-numerical displacement of each crack with limit (Domizio *et al*. 2017)

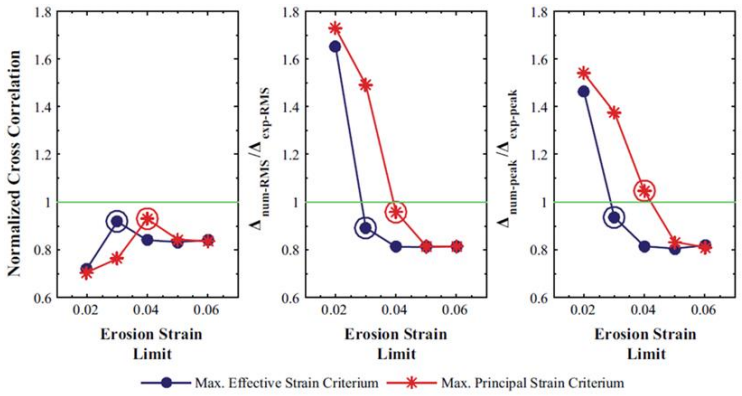

Fig. 5 Comparison indicators of experimental-numerical displacement of each erosion criteria (Domizio *et al*. 2017)

Table 2 Natural frequencies of the actual bridge

Mode	Modal Shape	Experimental Freq. (Hz)	Numerical Freq. (Hz)	Difference (%)
1	Lateral	3.68	3.68	0.00
2	Flexural vertical	4.24	4.22	-0.45
3	Torsional	5.47	5.45	-0.33

The influence of the flexibility of the soil was considered incorporating to the model a cylinder with the soil properties under each column. After some iterations, its diameter was defined as five times the diameter of the column, resulting in a cylinder of 4.00 m (Fig. 3(d)). The material of the soil was considered as linear elastic with a Young's modulus of 240 MPa.

The numerical model combines a total of 262,612 solid elements (8-node, under-integrated), 36,134 beam elements (2-node) and 20,351 shell elements (4-node). This huge number of 319K elements gives an idea of the high level of detail of the model and the large hardware resources required.

3.1 RC constitutive models

The constitutive model used to represent the concrete behaviour in RC frame is the Winfrith concrete model, developed by Broadhouse and Neilson (1987) and implemented in LS-DYNA software. This material model has been used by several authors to simulate concrete performance subjected to dynamic loadings (Domizio *et al*. 2019, Maazoun *et al*. 2017). The Winfrith concrete model takes into account a linear relation between stress and

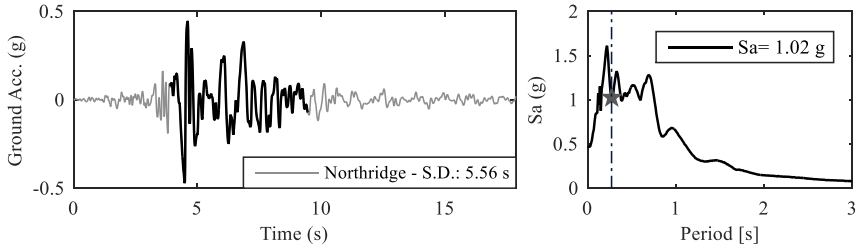

Fig. 6 Ground accelerations record and elastic response spectra, Northridge 1994

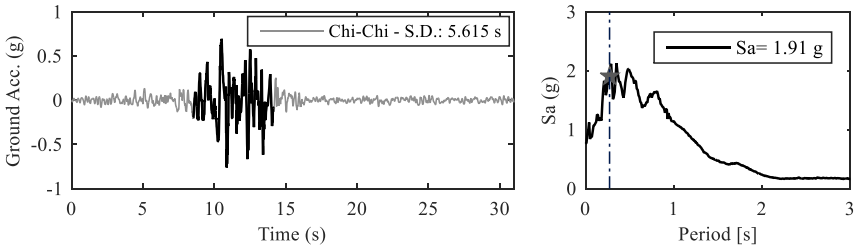

Fig. 7 Ground accelerations record and elastic response spectra, Chi-Chi 1999

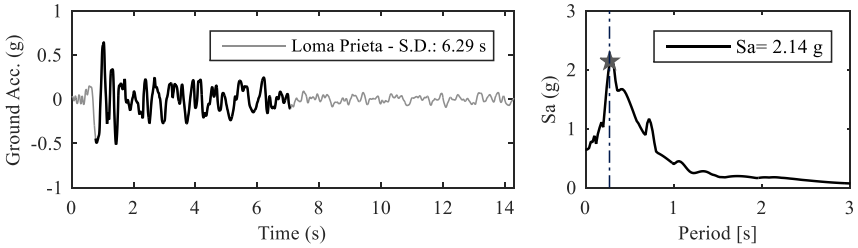

Fig. 8 Ground accelerations record and elastic response spectra, Loma Prieta 1989

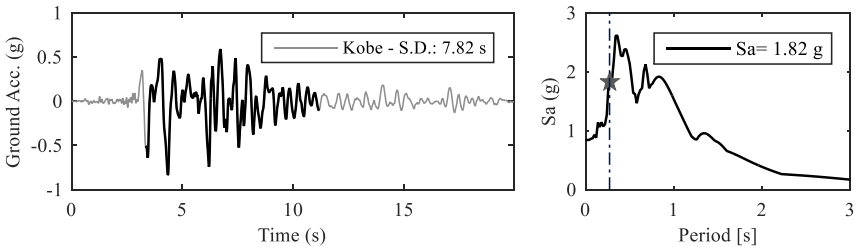

Fig. 9 Ground accelerations record and elastic response spectra, Kobe 1994

strains until the yielding surface *F*, defined by Ottosen (1977) criteria is reached.

$$F(I_1, J_2, cos3\theta) = a\frac{J_2}{f'^2_c} + \lambda\frac{\sqrt{J_2}}{f'_c} + b\frac{I_1}{f'_c} - 1 \qquad (1)$$

where I_1 is the first invariant of the main stress tensor, J_2 is the second invariant of the deviatoric stress tensor, f'_c is the characteristic strength of concrete to uniaxial compression, a and b are parameters that define the meridional yield surface shape, and λ is a function of Lode angle θ defined by the Eq. (2).

$$\lambda(cos3\theta) = \begin{cases} k_1 cos\left[\frac{1}{3}\cos^{-1}(k_2 cos3\theta)\right] & \text{for } cos3\theta \geq 0 \\ k_1 cos\left[\frac{\pi}{3} - \frac{1}{3}\cos^{-1}(-k_2 cos3\theta)\right] & \text{for } cos3\theta < 0 \end{cases} \qquad (2)$$

where k_1 and k_2 are parameters that define the shape of yield surface in the deviatoric plane. The parameters used in the numerical model are presented in Table 1.

In LS-DYNA, the non-linear behaviour of the Winfrith model is determined by four parameters in addition to the elastic characterization: uniaxial tensile strength f'_t, uniaxial compressive strength f'_c, maximum aggregate size and crack opening width (Table 1). Tensile failure is established when maximum principal stress at yield is greater than half the value of the tensile strength defined by the user. After there, strength decay with a linear relation as the crack develops. Finally, tensile strength takes a null value when the crack width equals the maximum value defined by the user.

Regarding steel, both longitudinal reinforcement and the transversal stirrups were modelled with a bilinear plasticity and kinematic hardening material. The material properties of steel rebars are presented in Table 1. All other structural RC members are considered as linear elastic materials (transversal girders and deck).

3.2 Calibration of the numerical model

Both the tensile and compressive strength of the concrete, as well as the maximum size of aggregates are known data of the concrete to be represented. While the maximum crack opening is a parameter associated with the fracture energy. Therefore, it requires an experimental calibration.

On the other hand, when real structures are subjected to ultimate loads, high localized nonlinearities take place in concrete due to stiffness degradation, cover spalling or crushing. It conducts to a heavy distortion in the finite

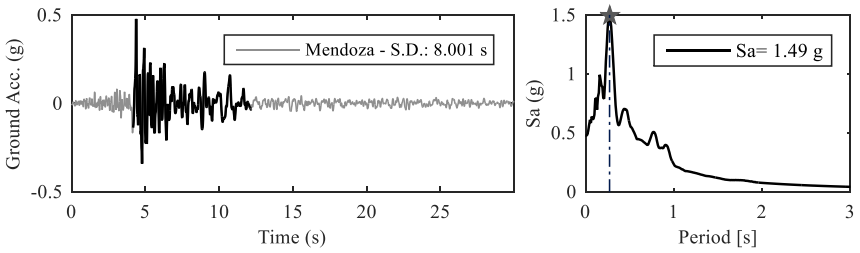

Fig. 10 Ground accelerations record and elastic response spectra, Mendoza 1985

Table 3 Seismic Records used in numerical simulation

Earthquake	Station	PGA (g)	SD (sec)	Sa (g)	Scale
Northridge 1994	WL Cany (270)	0.47	5.56	1.02	1.75
Chi-Chi 1999	CHY028 (N)	0.76	5.62	1.91	1.50
Loma Prieta 1989	Corralitos (000)	0.64	6.29	2.14	1.50
Kobe 1994	KJMA (0000)	0.83	7.82	1.82	2.00
Mendoza 1985	-	0.48	8.00	1.49	2.00

element mesh, causing numerical blocking and a consequent significant reduction of the time step, diminishing the computational efficiency. In order to avoid this negative aspect, an erosion algorithm is incorporated to the model thereby removing those elements that verify a specific requirement. It should be noted that erosion technique is only a numerical manipulation and has no physical meaning. Consequently, it also requires experimental calibration. A summary of the calibration process presented by Domizio *et al*. (2017) for maximum crack opening and erosion parameters is presented below.

3.2.1 Maximum crack opening

The dynamic response of 5 models with different values assigned to the studied parameter was analysed (0.02 mm, 0.05 mm, 0.10 mm, 0.15 mm and 0.20 mm). The numerical results were contrasted with the experimental test on a RC frame carried out by Elwood and Moehle (2003) in terms of horizontal displacements and base shear in the centre column of the frame.

To evaluate the degree of similarity between the experimental and the numerical responses, three indicators are defined: Normalized cross correlation R, root mean square (RMS) ratio and peak value ratio.

$$R = \frac{\sum_i a_{exp}[t_i] \cdot a_{num}[t_i]}{\sqrt{\sum_i a_{exp}[t_i]^2 \cdot a_{num}[t_i]^2}} \tag{3}$$

where R is the normalized cross correlation factor, a_{exp} and a_{num} are the experimental and numerical variables evaluated respectively in an instant of time t_i.

For the sake brevity, only the results for horizontal displacements are presented in Fig. 4. The similarity measures, in terms of RMS and peak values, are expressed as a ratio of the displacement obtained from the numerical models (Δ_{num}) to the displacement measured experimentally (Δ_{exp}). The parameter value that resulted in the highest degree of similarity is highlighted in the figure. In this case, this value corresponds to a crack width limit of 0.02 mm according to the three indicators used.

3.2.2 Erosion

There are several criteria to consider the erosion, some common based on deformations, stresses, damage, time step size, among others (Luccioni *et al*. 2013). Two strain-based erosion criteria were compared in this calibration process. The first criterion states that the element is removed from the numerical model if the effective strain exceeds a defined limit value. This effective strain is obtained through the following expression

$$\varepsilon_{eff} = \sum_{ij} \sqrt{\frac{2}{3} \varepsilon_{ij}^{dev} \varepsilon_{ij}^{dev}} \tag{4}$$

where ε_{ij}^{dev} are the components of the deviatoric strain tensor.

The second erosion criterion analysed uses the maximum principal strain to delete elements from the numerical model. This strain is obtained as the maximum eigenvalue of the strain tensor. Models with 5 different strain limits (0.02, 0.03, 0.04, 0.05 and 0.06) values were analysed with each erosion criterion. The numerical results were contrasted again with the experimental test by Elwood and Moehle (2003).

For the sake brevity, only the results for horizontal displacements are presented in Fig. 5. Limit strain values of 3% and 4% for the maximum effective strain and maximum principal strain erosion criteria respectively, produced the best agreement when compared with the experimental response. In this paper, the maximum effective criterion is used, with a value of 3%.

Finally, in order to obtain the elastic properties, the numerical model was calibrated by adjusting the natural frequencies of the actual bridge, obtained by experimental tests. Table 1 summarizes all the characteristics considered for each material of the numerical model. The numerical frequencies obtained through the modal analysis are compared with those obtained from experimental measurements, presented in a previous paper published by the authors (Nanclares *et al*. 2018), which are shown in Table 2.

The boundary conditions defined in the model consist of a restriction of displacements in the three directions in all

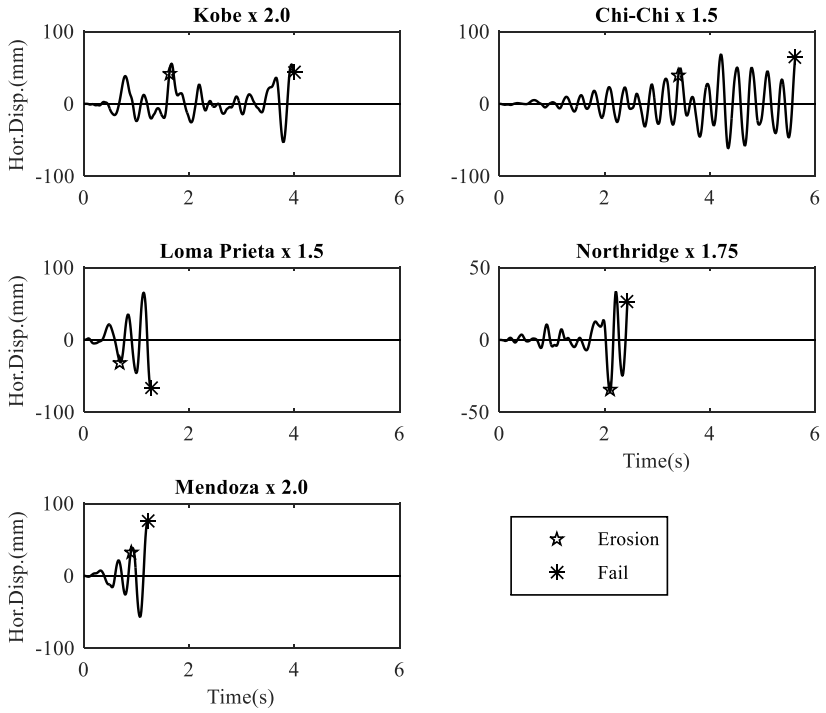

Fig. 11 Time history of horizontal displacements in control node

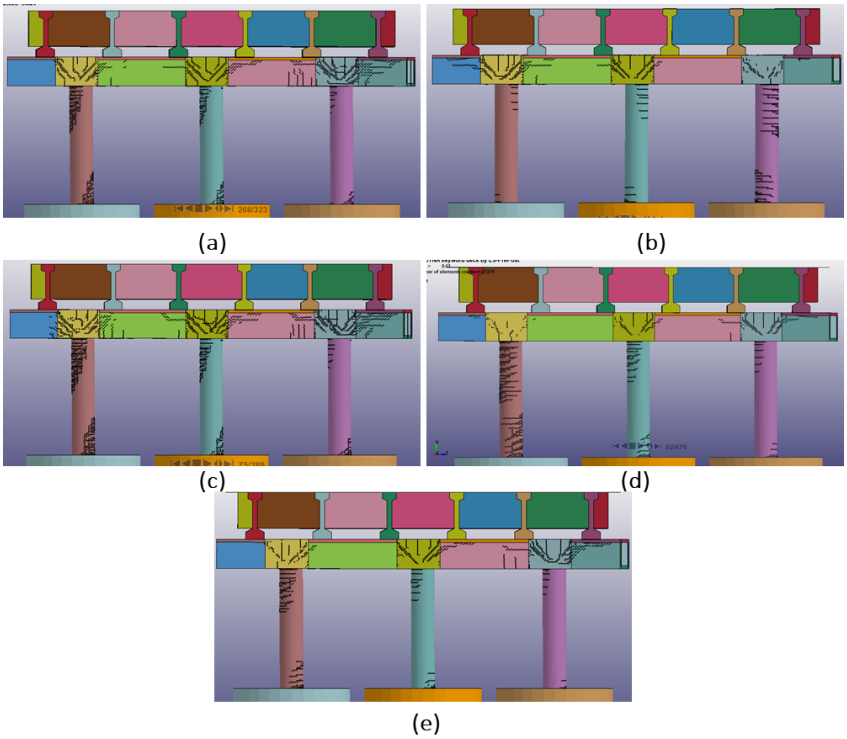

Fig. 12 Crack propagation in RC frame: (a) Northridge: Time = 2.07 sec; (b) Chi-Chi: Time = 1.57 sec; (c) Loma Prieta: Time = 0.74 sec; (d) Kobe: Time = 0.61 sec; (e) Mendoza: Time = 0.57 sec

the nodes that the external perimeter of the soil cylinder contains. On the other hand, at the ends of the longitudinal girders, the support in the abutments is considered as fixed supports. Non-structural elements are included as additional masses uniformly distributed, attached to the nodes of the deck.

4. External loads

A set of five actual seismic records with near-fault characteristics was selected, which are shown in Figs. 6-10. It means that the velocity records are strongly impulsive, with a relatively short duration, and a few pulses with high

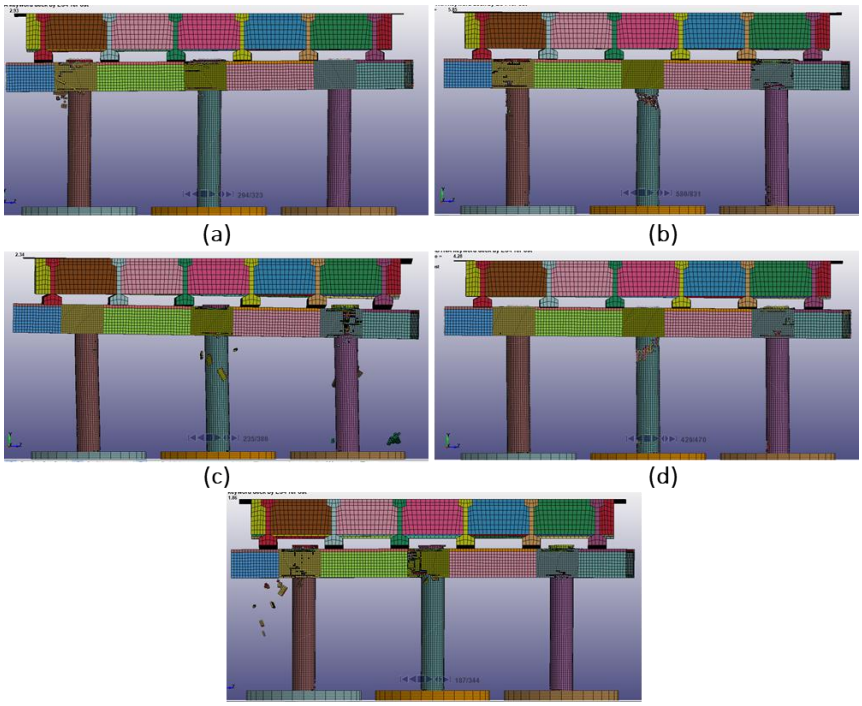

Fig. 13 Bridge collapse: (a) Northridge: Time = 2.93 sec; (b) Chi-Chi: Time = 5.85 sec; (c) Loma Prieta: Time = 2.34 sec; (d) Kobe: Time = 4.28 sec; (e) Mendoza: Time = 1.86 sec

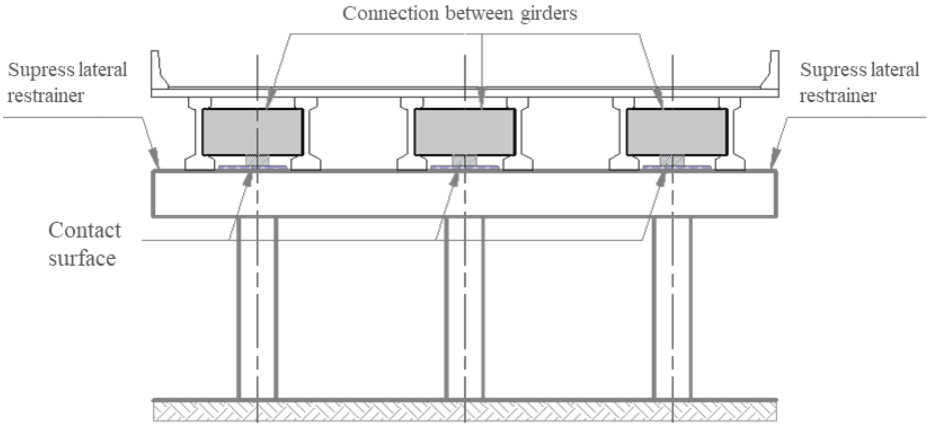

Fig. 14 Scheme of application of the sliding surface isolation system

amplitude and low frequency. On the other hand, the significant duration, defined as the time lapse comprehended between the release of 5% of the energy I_A, (Eq. (5)) up to 95%, was evaluated.

$$I_A = \frac{\pi}{2\,g}\int_0^{t_0} \ddot{u}\,(t)\,dt \tag{5}$$

where g is the acceleration of gravity and $\ddot{u}$ is the acceleration of the seismic record.

Each ground acceleration record was scaled by the factor indicated in Table 3, which ensure the bridge's collapse. Aforementioned seismic records were incorporated to the model as horizontal acceleration, in the transversal direction to the longitudinal axis of the bridge.

5. Numerical results

5.1 Structural response

Time history of horizontal displacements obtained in a control node located in the barycentre of the girder's frame is shown in Fig. 11. The time of erosion of the first element, and finally the moment in which the collapse of the structure is considered, is displayed in each curve.

5.2 Evaluation of failure mechanism

The crack pattern developed in the RC Frame during each seismic record is presented in Fig. 12. It is noteworthy that the piles show a typical flexural cracking state, in

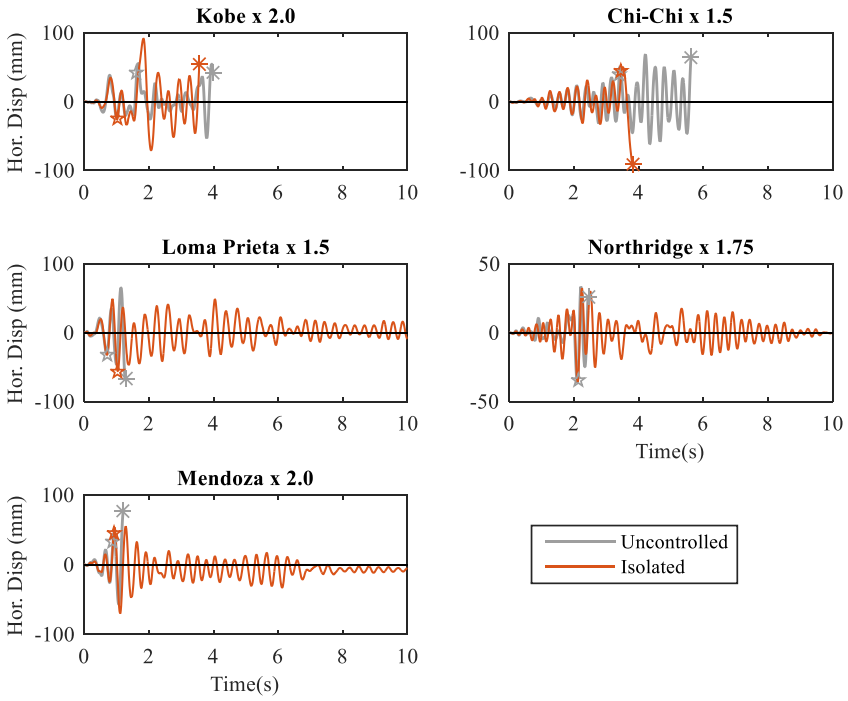

Fig. 15 Time history of horizontal displacements. Deck isolation

which both ends of the columns are subjected to tensile stresses in the opposite faces. Referring to beam, the presence of diagonal cracks in beam-to-column joints demonstrates the existence of significant shear stresses.

In all cases, structure collapse begins with the punching of head girder (Fig. 13). Only in the Chi-Chi (Fig 13(b)) and Kobe (Fig. 13(d)) earthquakes, the substructure shows the failure of columns at the top, due to a combination of bending moment and shear forces. However, these failure phenomena occur after breaking the girder by punching.

6. Passive vibration control systems

6.1 Deck isolation

The isolation technique represents one of the most currently implemented solutions to seismic protection to both bridges and buildings. The evolution of the isolation concept has been developed permanently and constantly to this day (Makris 2019). The essential purpose of this idea is to decouple a structure or part of it, from damaging effects of strong ground accelerations. This is achieved by a significant increase in the fundamental vibration period of the structure and a consequent decrease in the effective accelerations, all of which is caused by the insertion of additional deformable elements (Shahabi *et al*. 2020). The reduction in inertial forces is closely related to the increase in horizontal displacements of the structure as a rigid-body motion.

According to the purpose of this work, the isolation is incorporated through a frictionless contact surface, free to move in horizontal direction. This idealized assumption represents the extreme case in which the horizontal vibration of the deck does not introduce shear stresses on the frame.

The penalty method approach is adopted to model the contact interfaces between meshes because of its effectiveness and simplicity for explicit analysis. With this method slave nodes penetration is restricted via the imaginary normal interface springs between the shooting nodes and contact surfaces (LSTC 2017).

By virtue of the small seat length on the main girder that allows the deck to slide, it is decided to supress both lateral restrains (shown in Fig. 1(b)). In addition, the contact surface is relocated to coincide with the axis of each column. To achieve this, the main girders are grouped in pairs, by means of increasing the width of the transversal beam. With these modifications (Fig. 14), a double goal is sought: On one hand, the slider length available is increased. On the other hand, the shear stresses, introduced by the supports of the girders on each side of the column, are reduced.

The numerical results in terms of horizontal displacements of RC Frame are shown in Fig. 15. It is demonstrated that both Kobe (Fig. 15(a)) and Chi-Chi (Fig. 15(b)) earthquakes lead to the structure to collapse. The remaining simulations exhibit a large development of damage in the RC frame, even though collapse is avoided (Figs. 16(c)-(d)). It is noteworthy that the collapse mechanism is significantly modified compared to the uncontrolled response, as structural damage is developed in both ends of the columns instead of punching the head girder. In this case, due to the collapse mechanism, it is from more interest to study axial forces instead shear forces. Time history of axial force in left column is shown in Fig. 17. Important amplifications with respect to uncontrolled response are observed. As a first remark, it should be noted

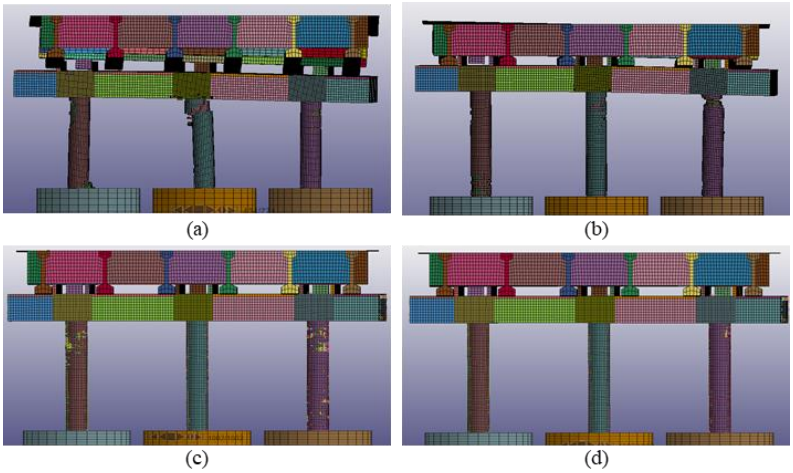

Fig. 16 Bridge response: (a) bridge collapse, Kobe: Time = 4.23 sec; (b) bridge collapse, Chi-Chi Time = 5.42 sec; (c) damaged RC frame, Loma Prieta: Time = 10 sec; (d) damaged RC frame, Mendoza: Time = 10 sec

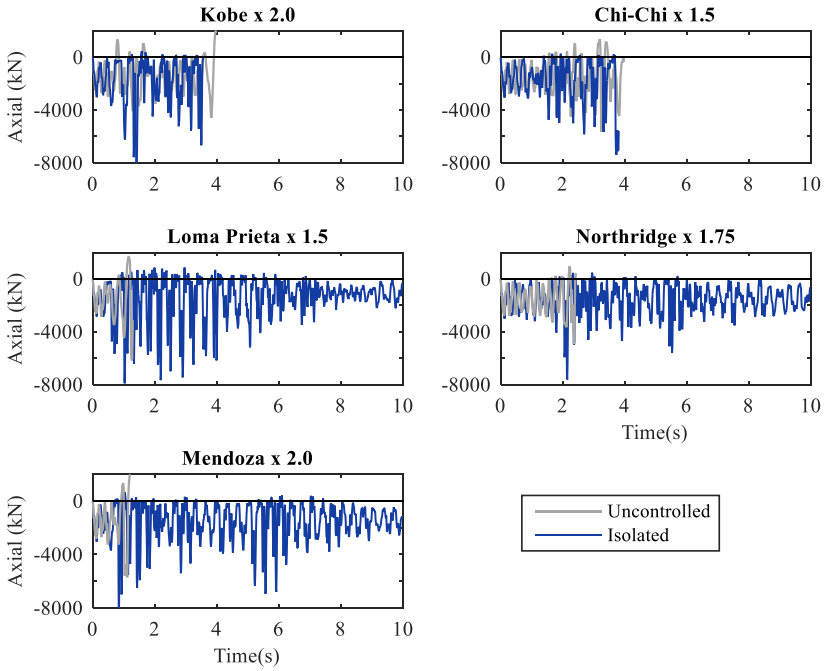

Fig. 17 Time history of axial force in left column. Deck isolation

Table 4 Frequencies of the isolated bridge

Mode	Modal shape	Frequency (Hz)
1	Lateral	0.909
2	Torsional of RC frame	3.607
3	Flexural	4.262
4	Horizontal RC frame	4.760

that axial forces increase in compression but decrease in tension. This is a direct implication of the change made in the contact condition. The ideal frictionless contact allows the deck to move in any horizontal direction and also permits separation between the two parts. This issue leads to an uplift of the girders in their supports, subsequently hitting the main girder of the frame, in an unexpected type of pounding to the piles. This explains the increase in the peak values in the time history of axial forces. In most papers in the literature, pounding actually occurred between the bridge girders and abutments (Bi and Hao 2013). An important finding of this work is the evidence of pounding between the girders and central frame, degrading the response of the columns.

This counterintuitive result, that isolating the deck does not prevent the bridge from collapsing, deserves an in-deep analysis. This analysis is separated in two items: dynamic characteristics and skewed geometry of the bridge.

6.1.1 Dynamic characteristics

When performing a modal analysis to the isolated bridge, the frequencies and modal shapes obtained are as

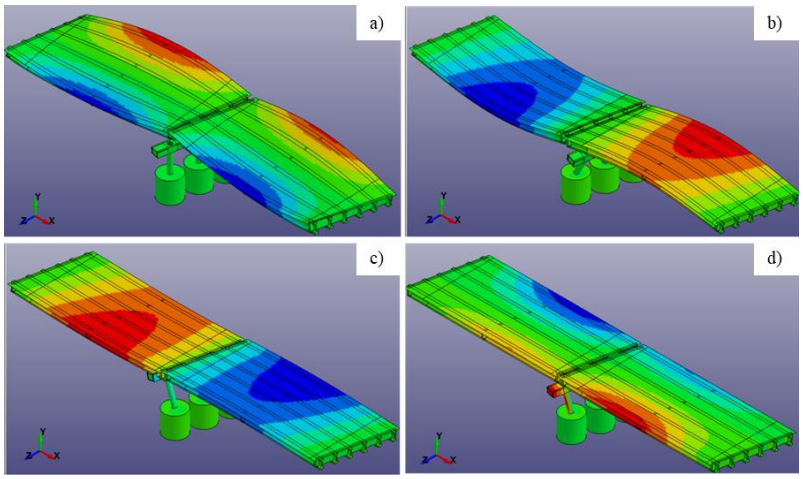

Fig. 18 First four modes of vibration of the isolated bridge: (a) lateral mode, $f = 0.909$ Hz; (b) torsion of the frame outside its plane, $f = 3.607$ Hz; (c) flexural mode, $f = 4.262$ Hz; (d) lateral mode of the frame, $f = 4.76$ Hz

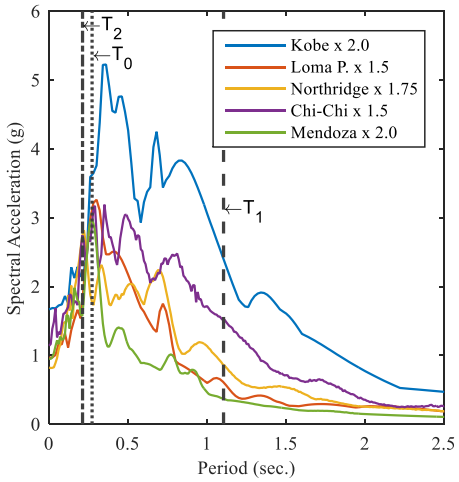

Fig. 19 Elastic response spectra of accelerations for each earthquake considered

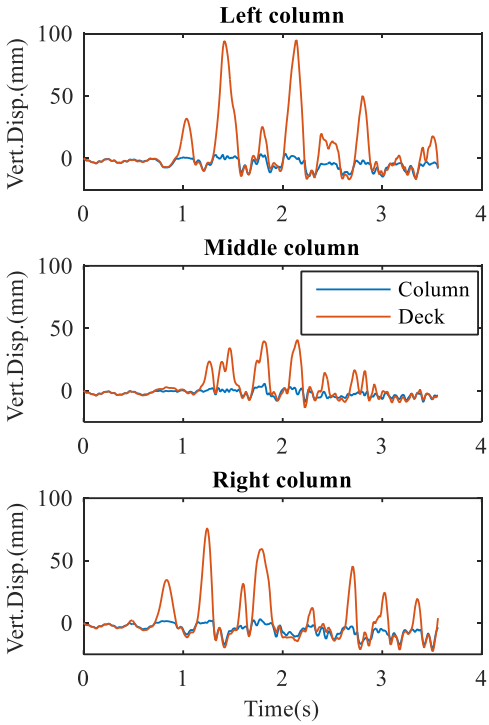

Fig. 20 Gap opening in surface contact for each column of the isolated bridge, Kobe earthquake

presented in Table 4 and depicted in Fig. 18. It can be observed that a new mode of vibration appears, which involves the vibration of the RC frame out of its plane. Furthermore, it is evident that the lateral displacement of the deck produces torsion around the longitudinal axis, generating uplifts in one side on the deck and descents on the opposite side.

The response spectra of seismic records are presented in Fig. 19, jointly with the main natural periods of the structure. The natural period of the uncontrolled structure was $T_0 = 0.27$ sec (Table 2). Although the natural period of the isolated deck increased considerably, $T_1 = 1.1$ sec, the frequency of the frame does not vary notably, $T_2 = 0.21$ sec. Thus, the horizontal accelerations do not decrease considerably (Fig. 19). Despite involving a minor mass in the dynamic response, the horizontal accelerations are strong enough to deteriorate the columns, even compromising the overall stability of the structure.

6.1.2. Skewed geometry of the bridge

The skewed geometry of the bridge produces an effect of torsion around the longitudinal axis. The consequence of this issue leads to an uplift of the girders in their supports, subsequently hitting the main girder of the frame, in an unexpected type of pounding between girders and central frame.

Comparing the vertical displacements of the deck with those of the frame, the aforementioned gap between the surfaces can be verified (Fig. 20). Further, this gap opening in the left column coincides with peak values of axial force in the right column, which could be seen in Fig. 21. Besides, it is highlighted that the maximum axial force values decrease due to the progressive degradation of the concrete. Although this aspect has been described for the

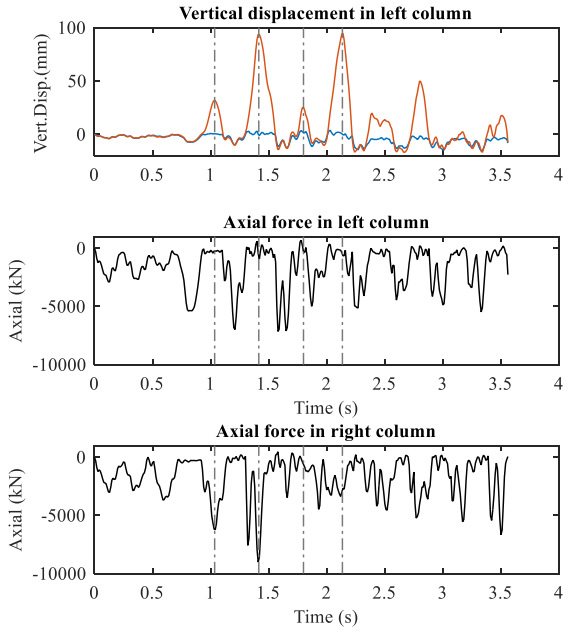

Fig. 21 Gap opening in contact compared with axial force in columns, Kobe earthquake

Kobe earthquake, it is a common feature of all simulations. For brevity, the analysis corresponding to the rest of the simulations is not shown in this work.

Then, the main reason that explains the collapse of the isolated bridge is found in the skewed geometry of the abutments, that introduce significant torsional actions around the longitudinal axis of the bridge. This well-known effect is aggravated by the skewed position of the intermediate RC frame, as shows the plan view presented in Figs. 1(c) and 3(d).

6.2 Metallic damper

In order to compare the deck isolation results with a classical passive system, a metallic damper is added to the studied structure. This type of device dissipates energy through the inelastic deformations of its metallic components. Metallic dampers work by reducing deformations from the combined effect provided by the device, adding stiffness and energy dissipation capacity in the structure.

In this paper, an arrangement as indicated in Fig. 22(a) is assumed. MDs were introduced in the model by means of a discrete element defined by an elastoplastic material with post-yielding hardening (Fig. 22(b)). The values of elastic stiffness, yielding force and post-yielding stiffness used in the simulations are extracted from a previous paper (Nanclares *et al*. 2018), in which an optimization of the design was carried out, in an effort to find high reductions in horizontal displacements with a moderate increase of base shear. The optimal values are: yielding force F_y = 550 kN, elastic stiffness K_e = 458.3 kN/mm and post-yielding stiffness K_{py} = 6 kN/mm.

The implementation in the numerical model is achieved by adding diagonal braces that concentrate the relative displacements of the frame in the middle height. These braces are considered as beam elements with elastic behaviour. Both upper and lower braces are connected by means of a discrete element with an elastic-plastic behaviour according to the optimal values aforementioned.

The time history of the horizontal displacements is presented in Fig. 23. It shows the dynamic response for each previously selected earthquake. It is outlined that not only the collapse of the structure is avoided, but also a significant reduction of the lateral displacement of the bridge is achieved.

On the other hand, the shear forces in the left pile are shown in Fig. 24. Shear forces are clearly increased with the incorporation of the device. This effect is predictable since the device reacts against the base of the column to develop its dissipating capacity, as Casciati *et al*. (2009) remark. This observation can be verified in all studied earthquakes, even though the collapse of the structure does not occur. Although the increase in base shear is an undesirable effect, the response of the bridge overall is improved and the column does not exceed its ultimate strength. The steel jacketing, which fixes the device, provides further improvement confining the concrete laterally, hence enhancing its mechanical behaviour.

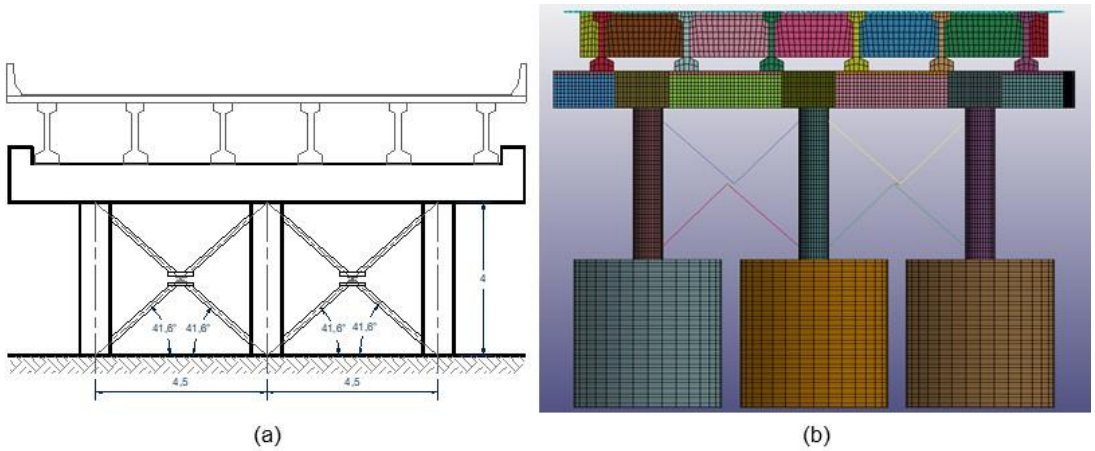

Fig. 22 (a) Schematic arrangement of MD in the bridge; (b) numerical model of the bridge with the MD

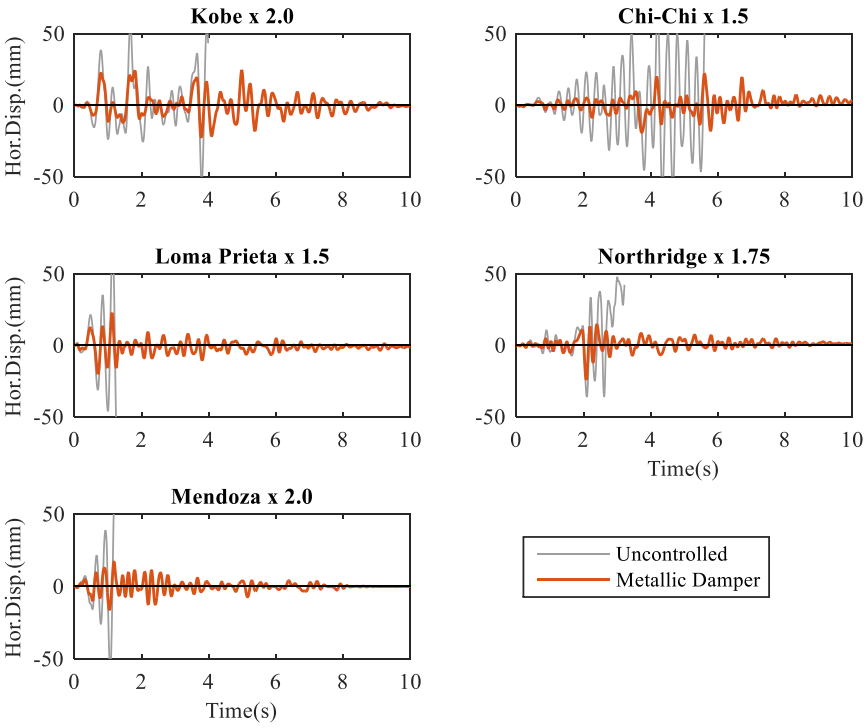

Fig. 23 Time history of horizontal displacement. Bridge with MD

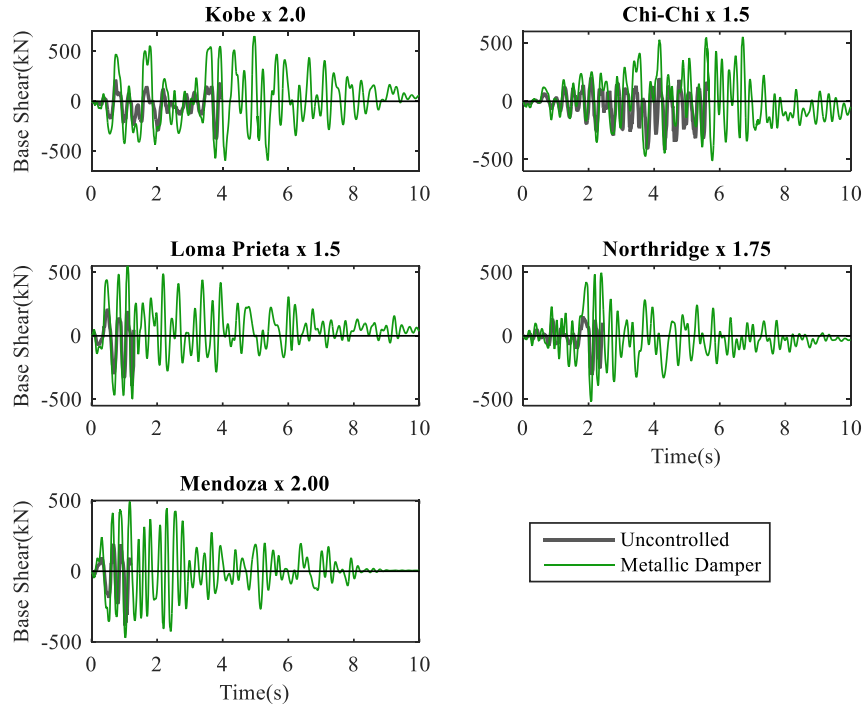

Fig. 24 Time history of base shear in left column. Bridge with MD

7. Discussion of the results

The full nonlinear RC model allows reproducing the nonlinear response until collapse of an actual RC bridge.

Metallic dampers prevent collapse in all the cases studied, while the isolation technique cannot avoid it, for some seismic records. As it can be seen, metallic dampers produce a decrease in horizontal displacements (Table 5), at the same time as shear forces in the base of columns are increased (Table 6). Despite the aforementioned, this fact does not imply a significant risk in the overall stability of the bridge, as these amplified forces do not reach the strength of the columns.

On the other hand, when considering the isolation of the

Table 5 Maximum horizontal displacement in time history simulation. Units in millimetres

Earthquake	Uncontrolled		Metallic damper		Deck isolation	
Northridge	55.5	100%	24.5	44%	91.7	165%
Chi-Chi	68.6	100%	21.9	32%	91.1	133%
Loma Prieta	68.1	100%	22.7	33%	55.9	82%
Kobe	36.2	100%	24.1	67%	35.8	99%
Mendoza	75.9	100%	17.1	23%	70.1	92%

Table 6 Maximum horizontal displacement in time history simulation. Units in millimetres

Earthquake	Uncontrolled	Deck isolation	
Northridge	4579,5	9017,8	197%
Chi-Chi	6603,8	7387,7	112%
Loma Prieta	6169,5	7907,3	128%
Kobe	4919,9	7615,0	155%
Mendoza	5713,2	8744,4	153%

Units in kN

deck, a slight decrease in horizontal displacements is obtained in those cases in which total collapse does not occur. The effectiveness of the isolation is seriously affected by the natural period of the frame, the skewed geometry of the bridge and its intermediate frame. When excited laterally, it experiences torsion of the deck and the main post-tensioned girders around the longitudinal axis. Therefore, it causes an uplift of the superstructure that generates a gap on the contact surface, which hits the girder in RC frame. The mentioned axial pounding on the piles, caused by longitudinal torsion can be distinguished in Fig. 17, by the presence of high peak values of compression and the lack of tension forces. This can be explained by the gap opening that occurs when the main girders are uplifted (Fig. 20).

8. Conclusions

A detailed nonlinear numerical model, calibrated against experimental tests, and subjected to different seismic records was used to reproduce the full nonlinear response until collapse of an actual RC bridge. Each one of these records was scaled to obtain the collapse of the bridge and to evaluate its behaviour, when seismic protective systems are included. To the best of the authors' knowledge, there is no such a full detailed nonlinear model published in the technical literature, with passive control systems, that studies the complete dynamic response of an actual bridge until collapse.

In the context in which this analysis was carried out, the implementation of a metallic damper significantly reduces the horizontal displacements and ensures the integrity of the structure from extreme seismic actions. Although shear forces in the column increase slightly compared with the uncontrolled response, the strength of the pile is not reached and mechanism of failure is not developed. The mentioned effect in shear forces is caused by the horizontal reaction necessary to provide the deformation in the metallic damper.

The isolation of the deck, which in principle seems to be the most effective solution to protect existing bridges, is inadequate for the case analysed, due to dynamic characteristic and its particular geometry. The close relationship between the behaviour of the bridge and its geometry, introduces forces that affect the structural integrity. Even when decoupling the mass belonging to the deck of the horizontal movement, the skew angle of the abutments introduces a longitudinal torsion that generate an unpredictable type of axial pounding in the columns. This new type of pounding generates high peak values in axial forces, which leads to the collapse of the structure.

It is worth mentioning that both the recognition of failure modes and the finding of vertical pounding between the girders and central frame in the isolation alternative, is only possible to identify through a highly detailed model such as the one presented. The fundamental role played by the non-linear constitutive model of materials and the defined erosion parameter are also highlighted, with the aim of visualizing the effects that are difficult to predict previously. Therefore, the importance of performing structural analysis with more sophisticated methods than the traditional ones is established. Likewise, the utility that these highly complex non-linear models represent to protect existing structures is emphasized.

Acknowledgments

The financial support of the CONICET is acknowledged. The technical documentation of the studied bridge supplied by Eng. Daniel Quiroga is also grateful. Special acknowledgements are extended to the reviewers of the first version of the paper because their useful suggestions led to improvements of the work.

References

Akbari, R. and Maalek, S. (2018), "A review on the seismic behaviour of irregular bridges", *Proc. Inst. Civ. Eng. Struct. Build.*, **171**(7), 552-580. https://doi.org/10.1680/jstbu.17.00081.

Bi, K. and Hao, H. (2013), "Numerical simulation of pounding damage to bridge structures under spatially varying ground motions", *Eng. Struct.*, **46**, 62-76. https://doi.org/10.1016/j.engstruct.2012.07.012.

Bi, K. and Hao, H. (2015), "Modelling of shear keys in bridge structures under seismic loads", *Soil Dyn. Earthq. Eng.*, **74**, 56-68. https://doi.org/10.1016/j.soildyn.2015.03.013.

Borón, P. and Dulinska, J.M. (2016), "Seismic performance of a reinforced concrete bridge under a sequence of seismic shocks using the concrete damage plasticity model", *Czasopismo Tech.*, **2016**(9), 15-29. https://doi.org/10.4467/2353737XCT.16.208.5957.

Broadhouse, B.J. and Neilson, A.J. (1987), "Modelling reinforced concrete structures in DYNA3D", *UK AEA*, **20**(8), 20025656.

Calvi, G.M., Kawashima, K., Billings, I., Elnashai, A., Nuti, C., Pecker, A., Pinto, P.E., Priestley, N.M.J., Rodriguez, M., Sarno, L., Franchin, P., Pietra, D. and Vanzi, I. (2007), *Seismic Bridge*

Design and Retrofit - Structural Solutions, Bulletin, USA. https://doi.org/10.35789/fib.BULL.0039.

Casciati, F., Faravelli, L. and Al Saleh, R. (2009), "An SMA passive device proposed within the highway bridge benchmark", *Struct. Control Health Monit.*, **16**(6), 657-667. https://doi.org/10.1002/stc.332.

Koem, C., Shim, C.S. and Park, S.J. (2016), "Seismic performance of prefabricated bridge columns with combination of continuous mild reinforcements and partially unbonded tendons", *Smart Struct. Syst. Int. J.*, **17**(4), 541-557. https://doi.org/10.12989/sss.2016.17.4.541.

Deng, L., Wang, W. and Yu, Y. (2016), "State-of-the-art review on the causes and mechanisms of bridge collapse", *J. Perform. Constr. Facil.*, **30**(2), 04015005. https://doi.org/10.1061/(ASCE)CF.1943-5509.0000731.

Di Sarno, L., Da Porto, F., Guerrini, G., Calvi, G.M., Camata, G. and Prota, A. (2019), "Seismic performance of bridges during the 2016 central Italy earthquakes", *Bull. Earthq. Eng.*, **17**(10), 5729-5761. https://doi.org/10.1007/s10518-018-0419-4.

Domizio, M., Ambrosini, D. and Curadelli, O. (2017), "Nonlinear dynamic numerical analysis of a RC frame subjected to seismic loading", *Eng. Struct.*, **138**, 410-424. https://doi.org/10.1016/j.engstruct.2017.02.031.

Domizio, M., Ambrosini, D. and Curadelli, O. (2019), "TMD effectiveness in nonlinear RC structures subjected to near fault earthquakes", *Smart Struct. Syst., Int. J.*, **24**(4), 447-457. https://doi.org/10.12989/sss.2019.24.4.447.

Dulinska, J.M. and Szczerba, R. (2013), "Assessment of concrete bridge performance under moderate seismic shock using concrete damage plasticity model", *Procedia Eng.*, **57**, 1319-1328. https://doi.org/10.1016/j.proeng.2013.04.166.

Elwood, K. and Moehle, J.P. (2003), "Shake table tests and analytical studies on the gravity load collapse of reinforced concrete frames", Ph.D. Dissertation, University of California, Berkley, USA.

He, X.H., Sheng, X.W., Scanlon, A., Linzell, D.G. and Yu, X.D. (2012), "Skewed concrete box girder bridge static and dynamic testing and analysis", *Eng. Struct.*, **39**, 38-49. https://doi.org/10.1016/j.engstruct.2012.01.016.

Hu, M., Han, Q., Du, X. and Liang, X. (2017), "Seismic collapse analysis of RC highway bridges based on a simplified multiscale FE modelling approach", *Shock Vib.*, **2017**, 5124767. https://doi.org/10.1155/2017/5124767.

Lee, K. and Yun, Y. (2008), "Parameter identification for nonlinear behavior of RC bridge piers using sequential modified extended Kalman filter", *Smart Struct. Syst., Int. J.*, **4**(3), 319-342. https://doi.org/10.12989/sss.2008.4.3.319.

Li, Z., Chen, Y. and Shi, Y. (2017), "Numerical failure analysis of a continuous reinforced concrete bridge under strong earthquakes using multi-scale models", *Earthq. Eng. Eng. Vib.*, **16**(2), 397-413. https://doi.org/10.1007/s11803-017-0389-6.

LSTC (2017), *LS-DYNA Keyword User's Manual*, Livermore Software Technology Corporation, USA.

Luccioni, B.M., Aráoz, G.F. and Labanda, N.A. (2013), "Defining erosion limit for concrete", *Int. J. Protect. Struct.*, **4**(3), 315-340. https://doi.org/10.1260/2041-4196.4.3.315.

Maazoun, A., Matthys, S., Vantomme, J., Belkassem, B. and Mourão, R. (2017), "Numerical prediction of the dynamic response of reinforced concrete hollow core slabs under blast loading", *Proceedings of the 10th European LS-Dyna Conference*, Salzburg, Austria 2017, May.

Makris, N. (2019), "Seismic isolation: Early history", *Earthq. Eng. Struct. Dyn.*, **48**(2), 269-283. https://doi.org/10.1002/eqe.3124.

Moharrami, M. and Koutromanos, I. (2017), "Finite element analysis of damage and failure of reinforced concrete members under earthquake loading", *Earthq. Eng. Struct. Dyn.*, **46**(15), 2811-2829. https://doi.org/10.1002/eqe.2932.

Nanclares, G., Ambrosini, D. and Curadelli, O. (2018), "Evaluation of classical reinforcement and passive control systems on a reinforced concrete bridge subjected to seismic loading", *Int. J. Lifecycle Perform. Eng.*, **2**(3-4), 189. https://doi.org/10.1504/IJLCPE.2018.10016092.

Ottosen, N.S. (1977), "A failure criterion for concrete", *J. Eng. Mech.*, **103**(4), 527-535.

Palermo, A., Liu, R., Rais, A., McHaffie, B., Andisheh, K., Pampanin, S., Gentile, R., Nuzzo, I., Granerio, M., Loporcaro, G., McGann, C. and Wotherspoon, L. (2017), "Performance of road bridges during the 14 November 2016 Kaikoura earthquake", *Bull. New Zealand Soc. Earthq. Eng.*, **50**(2), 253-270.

Schanack, F., Valdebenito, G. and Alvial, J. (2012), "Seismic damage to bridges during the 27 February 2010 magnitude 8.8 Chile earthquake", *Earthq. Spectra*, **28**(1), 301-315. https://doi.org/10.1193/1.3672424.

Schultz, A.E. and Gastineau, A.J. (2016), *Innovative Bridge Design Handbook*, Elsevier Inc, USA. https://doi.org/10.1016/B978-0-12-800058-8.00031-1

Shahabi, A.B., Ahari, G.Z. and Barghian, M. (2020), "Base isolation systems - a state of the art review according to their mechanism", *J. Rehabil. Civ. Eng.*, **8**(2), 37-61. https://doi.org/10.22075/JRCE.2019.16186.1306.

Wotherspoon, L., Bradshaw, A., Green, R., Wood, C., Palermo, A., Cubrinovski, M. and Bradley, B. (2011), "Performance of bridges during the 2010 Darfield and 2011 Christchurch earthquakes", *Seismol. Res. Lett.*, **82**(6), 950-964. https://doi.org/10.1785/gssrl.82.6.950.

FC